# Industrial ComFliTe Applications

Hans Bleecke and Bernd Stickan

Airbus Operations GmbH, Airbusallee 1, 28199 Bremen
{hans.bleecke,bernd.b.stickan}@airbus.com
http://www.airbus.com/

**Abstract.** This part shows two industrial applications of the CFD-CSM coupling capability in the FlowSimulator environment, which was developed in the ComFliTe project. The coupling of CFD and CSM is focused on static aeroelastic simulations, i.e. on the definition of the flight shape in cruise and in manoeuvres. The numerical methods used have been presented above by Stickan et al.

**Keywords:** CFD-CSM simulation, static aeroelasticity, FlowSimulator.

## 1 Analysis of Structural Flexibility in CFD-CSM Static Coupling Simulations

### 1.1 Introduction

This chapter describes the comparison of CFD-CSM static coupling simulations with two different representations of the structural model. The differences in flexibility effects are studied using the CFD-CSM FlowSimulator environment described above by Stickan et.al., section 2. The investigation was done for a generic full aircraft configuration at realistic flight conditions, shown in Fig. 1. The configuration is defined with lifting surfaces in jig shape for as well the CFD geometry as the finite element (FE) models. The CFD mesh is a Centaur mesh[1] generated with best-practice Airbus settings and contained 38 million mesh nodes.

### 1.2 FE Model Representations

The first representation of the structural model is a beam-like FE model, Fig. 2 (left). Therefore the wing is assumed to have rigid profiles in the direction of the wing ribs. The second representation is a fully flexible dynamic NASTRAN FE model with about 50.000 surface points, Fig. 2 (right).

The coupling spline, shown in Fig. 3 is based on surface splines for all lifting surfaces of the model, and rigid body splines for cockpit, and tail-cone, flap track fairings, as well as the engines.

[1] Centaur mesh generation software, http://www.centaursoft.com

N. Kroll et al. (eds.), *Computational Flight Testing*, Notes on Numerical Fluid Mechanics and Multidisciplinary Design 123,
DOI: 10.1007/978-3-642-38877-4_17, 

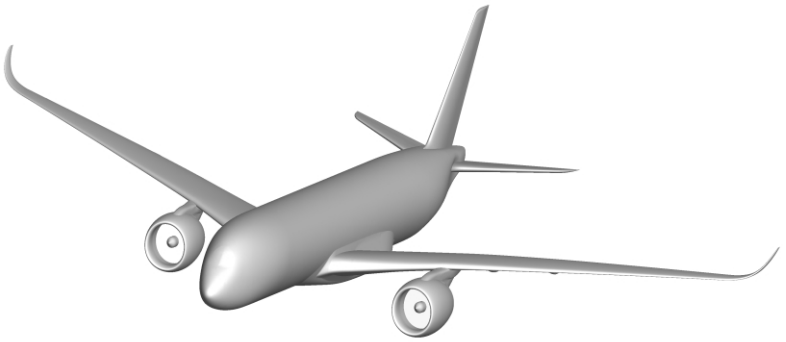

**Fig. 1.** Generic full aircraft configuration used for static CFD-CSM simulations

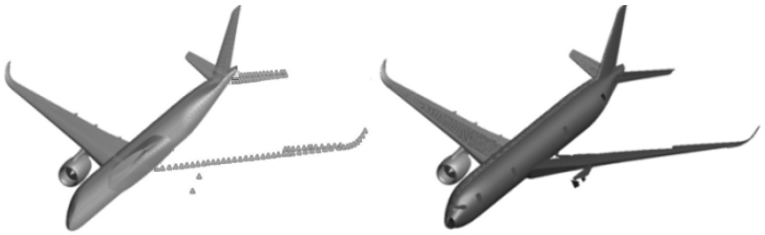

**Fig. 2.** The beam-like FE model (left) and the dynamic NASTRAN FE model (right)

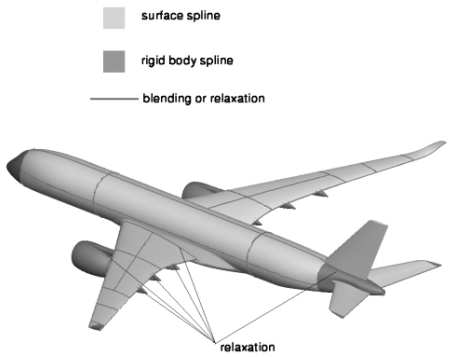


**Fig. 3.** Set-up of the surface coupling spline for the full aircraft configuration

### 1.3 Static CFD-CSM Simulations

The CFD solver TAU integrated in the FlowSimulator environment has been used to perform RANS simulations obtaining the aerodynamic forces on the aircraft surface. The process of interpolating the aerodynamic forces onto the structural model and obtaining the resulting deformation of the CFD surface mesh was described in detail above by Stickan et al.

The 1g-flight shape at horizontal steady flight has been determined for both FE model representations, in which the aircraft was not trimmed. The illustrative 1g-flight shape calculated with the CFD-CSM FlowSimulator process is shown in Fig. 4.


**Fig. 4.** Front view of the jig and calculated 1g-flight shape for a generic full aircraft configuration

The resulting wing deformation is represented as twist and bending distributions along the wingspan. First, the wing deformation for both FE models is calculated at the same angle of attack and representative flight conditions ($M = 0.85; h = 39000 ft$).

The resulting lift coefficient for the beam-like FE model is slightly lower than the lift coefficient of the NASTRAN dynamic FE model. Fig. 5 shows the comparison of span wise bending- and twist-distributions of the two FE models, compared to an Airbus standard method as a reference. A slight difference can be observed in the bending distribution of the two FE models, confirming the small $\Delta C_L$-effect.

Increasing the angle of attack by approximately $\Delta\alpha = 0.05^0$ for the simulation containing the beam like FE model results in the same lift coefficient for both CFD-CSM simulations. In this situation, the wings in both simulations carry the same load and the span wise twist and bending distribution is identical, see Fig. 6.

Fig. 7 shows the comparison of span wise pressure distributions ($\eta = 0.33$; 0.5; 0.66; 0.83) for both FE models at the same lift.

Whereas the pressure distribution on the lower surface is almost identical for both FE models, a remarkable difference is observed for the upper surface

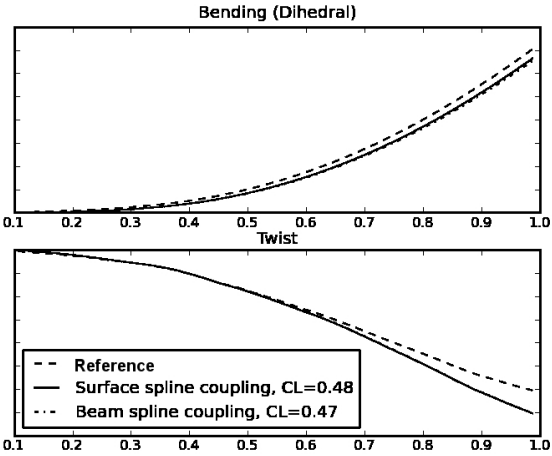


**Fig. 5.** Comparison of wing bending and twist for the same $\alpha$ at $M = 0.85; h = 39000ft$

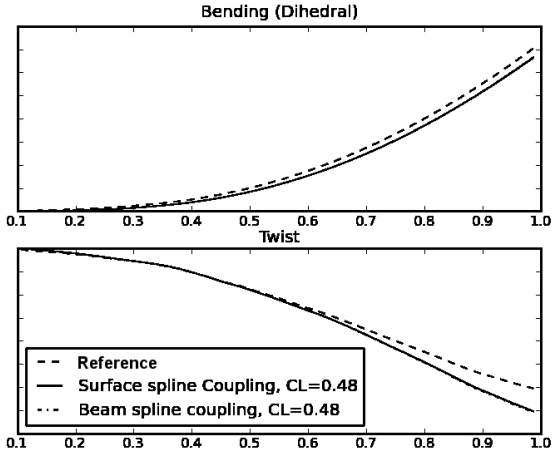


**Fig. 6.** Comparison of wing bending and twist for the same $C_L = 0.48$ at $M = 0.85; h = 39000ft$

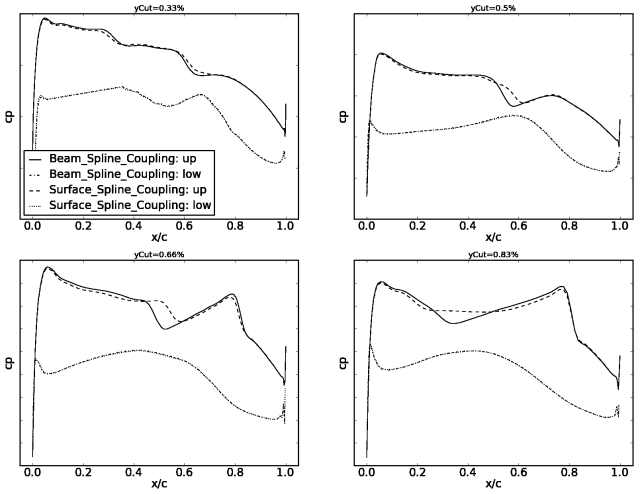


**Fig. 7.** Comparison of pressure distributions along wing span for both FE models and $C_L = 0.48$

pressure distribution. The shock position on the upper surface, calculated with the flexible NASTRAN FE model is substantially further downstream with respect to the beam-like model FE model for $\eta = 0.5$ and $\eta = 0.66$ As changes in local incidence across the span can be excluded from Fig. 6 , local cambering of the full flexible FE model on the upper surface must be responsible for the changes observed. The change in cambering for this model has been calculated with respect to the beam model with rigid profiles. In Fig. 8 this change is shown for different span wise locations. The largest, though very small cambering is a few millimeters and occurs approximately at midboard span positions.

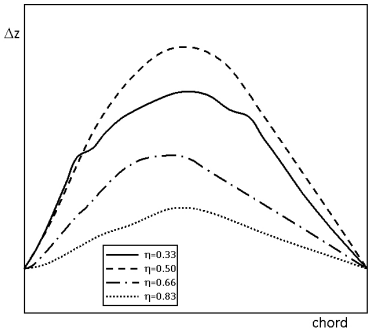


**Fig. 8.** Cambering of the upper surface along the wing span for the flexible FE model at $CL = 0.48$

Another observation is the linear behaviour of the camber line from the leading edge and the trailing edge towards midchord. This behaviour is related to the way in which the structural model has been prepared. As shown in Fig. 9 on the left, the CFD mesh (transparent) overlays the FE model, which is represented by the dark gray wing box. The connection of the leading and trailing edge to the wing box is represented with rigid body elements (RB elements), shown in Fig. 9.

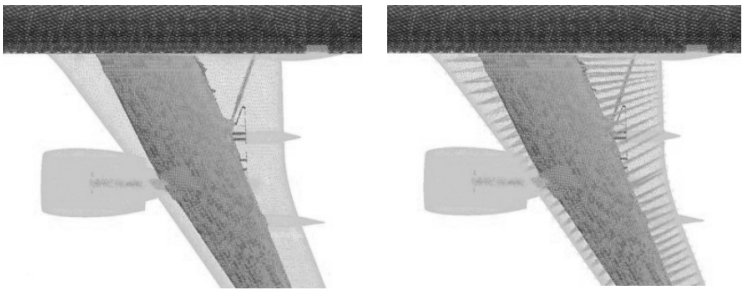

**Fig. 9.** FE and CFD model comparison without (left) and with (right) RB elements

These elements react as linear elements, explaining the linear parts in the cambering lines.

### 1.4 Conclusion

The ComFliTe project has enabled the capability development of static CFD-CSM simulations, which can be applied to high end industrial applications. The current representation of the dynamic FE model with RB elements is not capable of catching the right cambering of the profiles. This means that the change in aircraft wave drag will not be accurately captured in these kind of FE model approximation. An increase in FE model accuracy can be expected from an increase in complexity of the respective model, in which the high-lift slat and flap devices are resolved as surface models in the global FE model.

## 2 Fast Descent Manoeuvre

### 2.1 Introduction

A coupled simulation in the CFD-CSM FlowSimulator environment has been performed for the generic full aircraft configuration at Mach=0.85 using a load factor of 2.5 in order to approximate a fast descent manoeuvre. The calculations were based on a linear structural model and steady horizontal flight assumption. A full flex coupling was used to transfer forces and deformations between CFD and FE meshes. The higher load on the aircraft is compensated with a reduced

altitude. This altitude was chosen such that the dynamic pressure increased with the same factor as the load. In this way the simulation could be performed for the same target lift as for the conditions at $h = 39000ft$, since:

$$C_L = \frac{2.5W}{2.5\frac{1}{2}\rho V^2 S} = 0.47 \tag{1}$$

These conditions are met if the altitude is reduced from 39000ft to 18700ft.

### 2.2 Comparison of Static Simulations for 1g and 2.5g

A qualitative comparison of bending and twist shapes in relation to jig and 1g-flight is given in Fig. 10. The higher load additionally bends and twists the wing relative to the 1g-shape.

Fig. 11 shows the additional bend and twist distribution over the wingspan from 1g to 2.5g.

A qualitative impression of the pressure distribution for 1g-flight at $h = 39000ft$ is given in Fig. 12.

**Fig. 10.** Comparison of jig, 1g-, and 2.5g flight shape for a generic full aircraft configuration

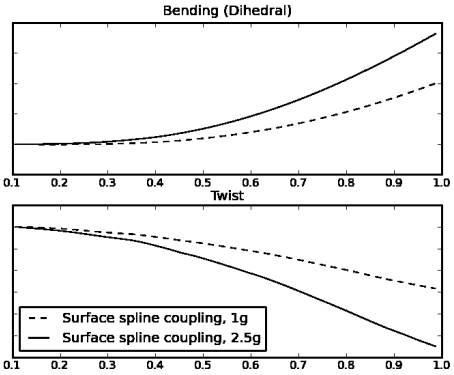


**Fig. 11.** The difference in bending and twist distribution over span for 1g- and 2.5g-flight shape

**Fig. 12.** The pressure distribution for the 1g-flight shape for $CL = 0.47$ at $M = 0.85; h = 39000ft$

If the altitude is lowered to $h = 18700ft$, the pressure distribution with the increased load of 2.5 is given in Fig. 13. A massive change in the shock system over the whole upper wing surface can be observed.

**Fig. 13.** The pressure distribution for the 2.5g-flight shape for $CL = 0.47$ at $M = 0.85; h = 18700ft$

### 2.3 Conclusion

The high load on the aircraft is calculated here using linear FE models, which become less accurate for large deformations, such as given here for the fast descent manoeuvre. The preparation of nonlinear NASTRAN models was not foreseen within the ComFliTe project, so that only the capability demonstration for these kind of simulations was shown successfully.